Chaos, Solitons & Fractals 70 (2015) 85–94

Contents lists available at ScienceDirect

Chaos, Solitons & Fractals

Nonlinear Science, and Nonequilibrium and Complex Phenomena

journal homepage: www.elsevier.com/locate/chaos

Quasi-synchronization dynamics of coupled and driven plasma oscillators

U.E. Vincent [a,b,*], S.O. Kareem [a], B.R. Nana Nbendjo [c], A.N. Njah [d]

[a] Department of Physical Sciences, Redeemer's University, P.M.B. 3005, Redemption City, Nigeria
[b] Department of Physics, Lancaster University, Lancaster LA1 4YB, United Kingdom
[c] Laboratory of Modeling and Simulation in Engineering and Biological Physics, Faculty of Sciences, University of Yaoundé I, PO Box 812, Yaoundé, Cameroon
[d] Department of Physics, University of Lagos, P.M.B 56 Akoka-Yaba, Lagos, Nigeria

ARTICLE INFO

Article history:
Received 6 August 2014
Accepted 5 November 2014

ABSTRACT

The dynamics of two coupled and periodically driven plasma oscillators is investigated in this paper. It is shown that the two oscillators exhibit rich dynamical transition to quasi-synchronized state. Stability and sufficient criteria for synchronization are analytically obtained using linear matrix inequality (LMI) and the Routh–Hurwitz criterion; and qualitatively characterized by the system's interaction energies. Moreover, the transition dynamics is rich with abundant complex bifurcation structures, including Hopf bifurcations. Based on the method of multiple time-scale, steady state equations for the vibration of the coupled oscillators have also been obtained, and bi-resonance induced by coupling at distinct frequencies are reported.

1. Introduction

Coupled nonlinear oscillators are ubiquitous in nature and well known for their rich varieties of dynamical behavior which includes higher-order chaos (hyperchaos), multi-stability of attractors and synchronization. While in general, synchronization phenomena are of fundamental importance in the study of biological, physical and technological problems [1–3]; multi-stability of attractors has been shown to accompany some synchronization transitions [4–6]. The history of synchronization dates back to the earlier observation of synchronization in the popular two clock pendula by Huygens [7]. A similar observation in the output of adjacent organ pipes was reported by Bleckman, whereby the individual effects of the pipes reduce collective output to either silence or peak [1,8]. These earlier studies were more specific to regular or periodic oscillations. In 1990, Pecora and Carroll [9] presented their results on the synchronization of identical chaotic systems which opened new directions of research activities in chaos synchronization [2]. The study of synchronized dynamics of chaotic systems derived its motivations from several potential applications in secure communication systems, time series analysis, modeling brain and cardiac rhythm activity and earthquake dynamics [1,2,10].

In recent years, full (identical/complete) synchronization have been extensively studied in the context of many specific problems. For general coupled chaotic systems with two phase space trajectories $x(t)$ and $y(t)$, the fulfillment of the condition, $\lim_{t\to\infty}\|x(t)-y(t)\|=0$ signifies full synchronization between $x(t)$ and $y(t)$. In reality and for many practical cases, the limit does not always approach zero asymptotically but a constant value, ϵ according to the inequality, $\lim_{t\to\infty}\|x(t)-y(t)\|<\epsilon$, implying imperfect complete or practical synchronization [8,11,12]; which in most cases arises from parameter mismatches between the two coupled systems. In practical situations, parameter mismatch is inevitable in synchronization implementations [13–15], and it has significant effects on the collective

* Corresponding author at: Department of Physics, Lancaster University, Lancaster LA1 4YB, United Kingdom.
E-mail address: u.vincent@lancaster.ac.uk (U.E. Vincent).

http://dx.doi.org/10.1016/j.chaos.2014.11.005
0960-0779/

behaviors of coupled systems. Loss of synchronization may take place in some cases [14]; while in other cases, complete synchronization can be maintained even with large parameter mismatch [15]. Imperfect complete synchronization phenomena are intriguing in nature as well as in practical situations and therefore deserves to be understood. Despite the huge results so far on other forms of synchronization, only few works have reported on quasi-synchronization due partly to its rare occurrence (See for instance Ref. [13,16–19]). More recently, renewed interest has been devoted to investigate this phenomenon and has been reported in [20–22]. In this paper, we report our observations of quasi-synchronization behavior in a model of coupled plasmas exhibiting chaotic dynamics.

Chaotic behavior in nonlinear plasma oscillations has been observed in several theoretical and experimental investigations [23–28]. For instance, the early work of Keen and Fletcher [23] showed that a marginal ion sound instability in a plasma behaves in a chaotic manner similar to that predicted by a Van der Pol type of nonlinear system. Hur et al. [24] observed period-doubling route to chaos in an ion beam going through dusts and electrons without collision; and bounded by two electrodes. Intermittent chaotic behavior in nonlinear three-wave model of space plasma was reported by Miranda et al. [25]. Sheridan [26] reported experimental observation of chaotic dynamics in a complex (dusty) plasma of three particles [27]. Recently, Enjieu-Kadji et al. [29,30] showed that the plasma oscillation maybe modeled as a nonlinear anharmonic oscillator of the Duffing-type displaying varieties of chaotic domain; and more recently considered chaos control problem for the same system [31]. Earlier investigations on the problem of chaos suppression in plasmas systems were experimentally carried out by Bezruchko et al. [32] and Koronovski et al. [33] in which by tuning the frequency of the external signal, chaos suppression was realized. In another related investigation, Viana et al. [28], analyzed the fractal structures of nonlinear plasma, emphasizing that fractals appear in certain applications in plasma physics, like the magnetic field line behavior in tokamaks with ergodic limiters. Viana et al. [28] further demonstrated the observable consequences of fractal structures in terms of the transport properties in the plasma edge of tokamaks and also discussed the role of the fractal structures in the understanding of mesoscale phenomena in plasmas.

Notwithstanding the increasing interest in plasma chaos research, only few studies have been devoted to the investigation of chaos synchronization in a nonlinear plasmas [34–37]. For instance Filatov et al. [35] investigated chaotic synchronization regimes for coupled spatially extended beamplasma Pierce systems and observed different synchronization regimes, namely phase synchronization, generalized synchronization, time-scale synchronization and complete synchronization. Similarly, an impulsive synchronization was employed by Li et al. [36] to realize chaos synchronization in a laser plasma system.

In this paper, we investigate the synchronization behavior of two linearly coupled plasma oscillators with a single external periodic driving. The single periodic forcing could be realized using some physical mechanism such as an externally applied electric field or an ultraviolet light. For instance, by means of photodetachment, ultraviolet light which can extract electrons from materials can be used as an external force to control the charge transport on a dust particle. This is because, it is well known that the transport of dust particles into plasma is proportional to the dust charge and the coagulation of small particles into larger ones due to the attraction or repulsion between charged particles through the coulomb potential (See Ref. [29] and references therein). In general, nonlinear systems with single external periodic driving exhibit varieties of nontrivial complex dynamics [38,39], including the possibility of mode locking phenomenon occurring at rational multipliers of driving frequency [2], among others. These are relevant nonlinear characteristics which are of immense practical applications, in areas such as optical tomography as well as communications [40]. Here, we report the occurrence of quasi-synchronization phenomenon in two coupled and driven plasma oscillators, in which the defining limit of synchronization is bounded within a definite small region around zero. i.e. $\lim_{t\to\infty}\| x(t)-y(t)\| = \epsilon \neq 0$. We derive sufficient synchronization criteria using linear matrix inequality (LMI). Although LMI is a well established method for determining the stability and synchronization threshold for linearly coupled systems, including oscillators with periodic and parametric driving (See for instance [41–46,4–6]), however, previous LMI-based approaches assume a mutual and identical external forcing on the oscillators, which eliminates the effect of periodic forcing on chaos synchronization criteria. We show explicitly that the external forcing parameters, which hitherto has been neglected, plays significant role in the robustness of the criteria.

Furthermore, we also report coupling-induced nonlinear dynamics associated with quasi-synchronization, namely complex bifurcation structures, with co-existing attractors and multiple resonances. The rest of the paper is organized as follows: In the next section, we describe our model system and obtain the synchronization criteria in Section 3. In Section 4, the transition to synchronization is examined. Section 5 is concerned with coupling-induced resonances. The paper is concluded in Section 6 with summary.

2. System description

Most of the models of plasma oscillations are concentrated on unmagnetized and collisionless dusty plasma, made up of electrons, ions and dust grains. They are usually characterized by micron or submicron sized dust particles (See Ref [47], and references therein). In dusty plasma, the dust grain charge is variable, and capable of causing significant modification on the plasma's properties, including its dissipative and nonlinear properties [47,48]. Here, we consider magnetized plasma, whose particle species form separate conducting fluids. The dynamics of this type of plasma has been extensively studied [29–31]. It consists of two interpenetrating fluids of positive ion (i) with charge $+e$ and electron (e) with charge $-e$. The Eulerian equations can be written as:

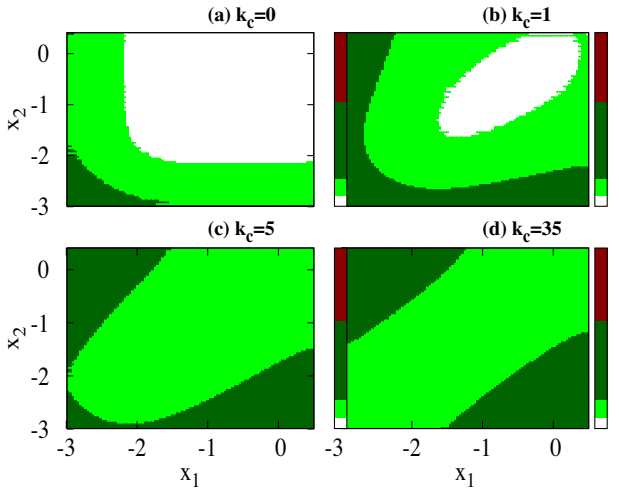

Fig. 1. The equipotential contour plots of $V(x_{1,2})$ for $\omega = 1, \kappa = 3.05, \delta = 1.5$ and $F = 0$. The colors evolves from white (minima) to dark green (maxima): (a) No interaction, $k_c = 0$, (b) weak coupling, $k_c = 1$, (c) moderate $k_c = 5$, (d) strong coupling, $k_c = 35$. (For interpretation of the references to color in this figure caption, the reader is referred to the web version of this article.)

$$\begin{aligned} &n_\alpha M_\alpha \frac{dv_\alpha}{d\tau} = n_\alpha q_\alpha (E + v_\alpha \times B - \mu J) - \Delta P_\alpha, \\ &\frac{\partial n_\alpha}{\partial \tau} + \Delta \cdot (n_\alpha v_\alpha) = S, \\ &\frac{d}{d\tau}(P_\alpha n_\alpha^{-\gamma}) = 0, \end{aligned} \tag{1}$$

where the effect of ionization or large amplitude vibrations in the plasma is denoted by S, α is the indexing for each of the species (i and e), n_α is the density with respect to the species; v_α and P_α represent their velocity and pressure, respectively, γ is the specific heat ratio, and $\mu_\alpha = M_\alpha v_\alpha / n_\alpha e^2$ is the resistive collision with v_α being the collision frequency. M_α denotes the mass of each specie α. Recently, Enjieu et al. [29–31] showed explicitly that the plasma oscillation maybe modeled as a nonlinear anharmonic oscillator of the Duffing-type as follows:

$$\frac{d^2 n_1}{d\tau^2} + (v_i + 2\lambda + 3\mu n_1^2)\frac{dn_1}{d\tau} + \omega^2 n_1 + v_i(\lambda n_1^2 + \mu n_1^3) = F_0 \cos\Omega t. \tag{2}$$

Re-defining the variables in Eq. (2) as $t = \omega_0 \tau$, $n_1 = \left(\frac{v_i + 2\lambda}{3\mu}\right)x = \Xi x$, $\epsilon = \frac{v_i + 2\lambda}{\omega_0}$, $\kappa = \frac{v_i \lambda \Xi}{\omega^2}$, $\delta = \frac{v_i \mu \Xi^2}{\omega_0^2}$, $F = \frac{F_0}{\Xi \omega_0^2}$ and $\Omega = \frac{\omega}{\omega_0}$, Eq. (2) in dimensionless form now reads

$$\ddot{x} + \mu(1 + x^2)\dot{x} + \frac{dV(x)}{dx} = 0; \tag{3}$$

where $V(x)$ is the plasma potential given as

$$V(x) = \sum_{j=2}^{4} \frac{\beta_j}{j} x^j - xF\cos\Omega t \tag{4}$$

and $\beta_2 = \omega^2, \beta_3 = \kappa$ and $\beta_4 = \delta$; the dots represent the differentiation with respect to time (t), μ, ω, Ω and F are the damping coefficients, fundamental frequency, forcing frequency and amplitude of the external force respectively, κ and δ are quadratic and cubic nonlinearity parameters, respectively.

Here, we consider two coupled plasma oscillators in a perturbed two-dimensional potential given as

$$V(x_{1,2}) = \sum_{j=2}^{4} \frac{\beta_j}{j}\left(x_1^j + x_2^j\right) + V_p(x_{1,2}) - x_1 F\cos\Omega t, \tag{5}$$

where $V_p(x_{1,2}) = \frac{k_c}{2}(x_2 - x_1)^2$ is a perturbation corresponding to the difference between the charge densities, k_c being the strength of the interaction. The last term in the potential (5) ensures that only a single external periodic forcing is applied to the system. Consequently, their equation of motion reads,

$$\ddot{x}_{1,2} + \mu\left(1 + x_{1,2}^2\right)\dot{x}_{1,2} + \frac{dV(x_{1,2})}{dx_{1,2}} = 0. \tag{6}$$

For the purpose of this study, we use the same set of system potential parameters as in Ref. [29], namely $\omega = 1, \kappa = 3.05$ and $\delta = 1.5$ and plot the 2D plasma potential (5) as shown in Fig. 1 for four different values of k_c and $F = 0$. The points around the minima and maxima of $V(x_{1,2})$ are marked with white and dark-green colors, respectively. In the absence of external forcing and for $k_c = 0, V(x_{1,2})$ is a bounded double-well asymmetric potential as shown in Fig. 4(a), with two minima located at $(x_1, x_2) = (0, 0)$ and $(-1.65, -1.65)$, respectively. As k_c increases, so that the difference between the charge densities of the two oscillators is negligible, the heights of $V(x_{1,2})$ collapses, opening up a valley along the diagonal, in which the two oscillators may most likely share in their synchronized states.

3. Stability and synchronization criteria

In this section, we would employ the Linear matrix inequalities (LMI) and Routh–Hurwitz criterion to obtain a sufficient criteria for global synchronization. Consider the following coupled plasmas derived from Eq. (6):

$$\ddot{x}_1 = -\mu(1+x_1^2)\dot{x}_1 - \frac{dV(x_{1,2})}{dx_1}, \tag{7}$$

$$\ddot{x}_2 = -\mu(1+x_2^2)\dot{x}_2 - \frac{dV(x_{1,2})}{dx_2}. \tag{8}$$

By letting $\dot{x_1} = y_1$ and $\dot{x_2} = y_2$ the second order differential equations (7) and (8) are expressed as systems of first-order differential equations with variables (x_1, y_1) and (x_2, y_2), respectively. In compact matrix form each system in Eqs. (7) and (8) may be written as:

$$\dot{\mathbf{X_1}} = \mathbf{AX_1} + \mathbf{f}(\mathbf{X_1}) + m(t) - \mathbf{U}, \tag{9}$$

$$\dot{\mathbf{X_2}} = \mathbf{AX_2} + \mathbf{f}(\mathbf{X_2}) + \mathbf{U}, \tag{10}$$

where $\mathbf{A} = \begin{pmatrix} 0 & 1 \\ -\omega^2 & -\mu \end{pmatrix}$, $\mathbf{X_1} = (x_1, y_1)^T \in \mathbf{R}^2$, $\mathbf{X_2} = (x_2, y_2)^T \in \mathbf{R}^2$, $\mathbf{f}(\mathbf{X_1}) = \begin{pmatrix} 0 \\ -(\mu y_1 + \kappa + \delta x_1)x_1^2 \end{pmatrix}$, $\mathbf{f}(\mathbf{X_2}) = \begin{pmatrix} 0 \\ -(\mu y_2 + \kappa + \delta x_2)x_2^2 \end{pmatrix}$, $m(t) = F\cos\omega t, \mathbf{U} = \mathbf{k_c}(x_1 - x_2)$, $\mathbf{k_c} \in \mathbf{R}^{2\times 2}$. Defining the error between Eqs. (9) and (10) as $\mathbf{e} = \mathbf{X_1} - \mathbf{X_2}$, we obtain the error dynamics

$$\dot{\mathbf{e}} = (\mathbf{A} - 2\mathbf{k_c} + \mathbf{Q}(t))\mathbf{e}, \tag{11}$$

where

$$\mathbf{Q}(t) = \begin{pmatrix} 0 & 0 \\ q(t) & 0 \end{pmatrix}; \quad q(t) = \frac{q_\dagger + m(t)}{x_1 - x_2}. \tag{12}$$

$q_\dagger = \mu(x_2^2 y_2 - x_1^2 y_1) + \kappa(x_2^2 - x_1^2) + \delta(x_2^3 - x_1^3)$. We assume that the attractors in each subsystem are bounded within the regions Γ and Λ, respectively; requiring that the maximum, $max|x_1| \leqslant \rho$, where $|x_1| \geqslant |x_2|$ and that global synchronization is implied if there exist a $\tau \geqslant t_0$ for which $\lim_{t\to\infty}\|\mathbf{X_1}(t) - \mathbf{X_2}(t)\| \leqslant \epsilon \forall t > \tau$; and that the synchronization is independent of initial conditions [7,16,31]. Following Ref. [4], it is easy to show that Eq. (12) may be written as

$$|q(t)| \leqslant \mu\rho^2 + 2\kappa\rho + 3\delta\rho^2 + \frac{|F|}{2\rho}. \tag{13}$$

If the control (coupling) matrix $\mathbf{k_c} \in \mathbf{R}^{2\times 2}$ is defined as

$$\mathbf{k_c} = \begin{pmatrix} k_{11} & k_{12} \\ k_{21} & k_{22} \end{pmatrix}, \tag{14}$$

then, the following theorem holds:

Theorem 1. *Suppose the coupling matrix (14) is chosen such that Eqs. (15) and (16) are satisfied, then the coupled plasmas (7) and (8) achieves global synchronization.*

$$k_{11} + k_{22} + \mu > 0, \tag{15}$$

$$4k_1 1(k_2 2 + \mu) > P_\omega, \tag{16}$$

where
$P_\omega = \left(|1 - k_{12} - k_{21}| - \omega^2 + \mu\rho^2 + 2\kappa\rho + 3\delta\rho^2 + \frac{|F|}{2\rho}\right)^2$.

Proof. The stability theory related to the linear time-varied systems requires that global synchronization is achieved if matrix, $\mathbf{G} \in \mathbf{R}^{2\times 2}$, defined in Eq. (14) is negative definite.

$$\mathbf{G} = \begin{pmatrix} -2k_{11} & h \\ h & -2(k_{22} + \mu) \end{pmatrix}, \tag{17}$$

where $\mathbf{G} = (\mathbf{A} - \mathbf{K_c} + \mathbf{Q}) + (\mathbf{A} - \mathbf{k_c} + \mathbf{Q})^\mathbf{T}$ and $h = q(t) - \omega^2 - (k_{12} + k_{21}) + 1$. Applying the Routh–Hurwitz criterion to the eigenvalue equation of Eq. (17), one obtains:

$$k_{11} + k_{22} + \mu > 0, \tag{18}$$

$$4k_{11}(k_{22} + \mu) - q(t) - \omega^2 - (k_{12} + k_{21}) + 1 > 0. \tag{19}$$

Using (13) in (19) we have,

$$|1 + q(t) - \omega^2 - (k_{12} + k_{21})| \leqslant |1 - \omega^2 - (k_{12} + k_{21})| + |\mu\rho^2 + 2\kappa\rho + 3\delta\rho^2| + \frac{|F|}{2\rho}. \tag{20}$$

Substituting Eq. (20) in Eq. (19), Eqs. (13) and (14) become Eqs. (15) and (16). This ends the proof. □

In order to obtain an explicit synchronization criteria which depends on the systems' parameters, we first consider the following corollaries based on Theorem 1.

Corollary 1. *If the coupling matrix is chosen as* $\mathbf{k_c} = \begin{pmatrix} k_1 & 0 \\ 0 & k_2 \end{pmatrix}$, *(15) and (16) may be written as*

$$k_1 + k_2 + \mu > 0, \tag{21}$$

$$4k_1(k_2 + \mu) > \left(|1 - \omega^2 + |\mu\rho^2 + 2\kappa\rho + 3\delta\rho^2| + \frac{|F|}{2\rho}\right)^2, \tag{22}$$

which guarantees global synchronization.

Corollary 2. *If the coupling matrix is chosen as* $\mathbf{k_c} = \begin{pmatrix} k_c & 0 \\ 0 & k_c \end{pmatrix}$, *then (22) is implies that*

$$k_c > \frac{-\mu + \sqrt{\mu^2 + (|1 - \omega^2 + q|)^2}}{2}. \tag{23}$$

Corollary 2, given by Eq. (23) gives the criteria for the synchronization of the coupled systems (7) and (8).

Next, we illustrate the synchronization process by numerical simulation of the coupled systems (7) and (8). The fourth-order Runge Kutta algorithm has been used to obtain our numerical results. Unless otherwise stated, all simulations were carried out with the following parameters fixed: $\mu = 0.02, \omega = 1, \kappa = 3.05, \delta = 1.5$, and $F = 22.0$; and starting with initial conditions, $(x_1, \dot{x_1}) = (0, 0.5), (x_2, \dot{x_2}) = (1.5, 2.5)$. First, we obtain the threshold coupling, k_c^{th}, which is an important synchronization parameter that is of general interest. From the boundedness condition, the limiting constant $\rho = 3.0$, so that an estimate of k_c directly from (23) gives the synchronization threshold, $k_c^{th} \approx 31.31$ – a minimum value of k_c for which the $\lim_{t\to\infty}\|x_2(t) - x_1(t)\| < \epsilon \neq 0$ is guaranteed. Note that the smaller the value of ϵ, the closer quasi-synchronization is to be equivalent to complete synchronization. For $k_c = 0$ which corresponds to the uncoupled case the two oscillators are independent running dynamical systems - chaotic and limit cycle oscillators, respectively (See Fig. 5(a)). The detail dynamics for the driven part has been presented by Enjieu Kadji et al. [29]. Fig. 2 shows the error dynamics

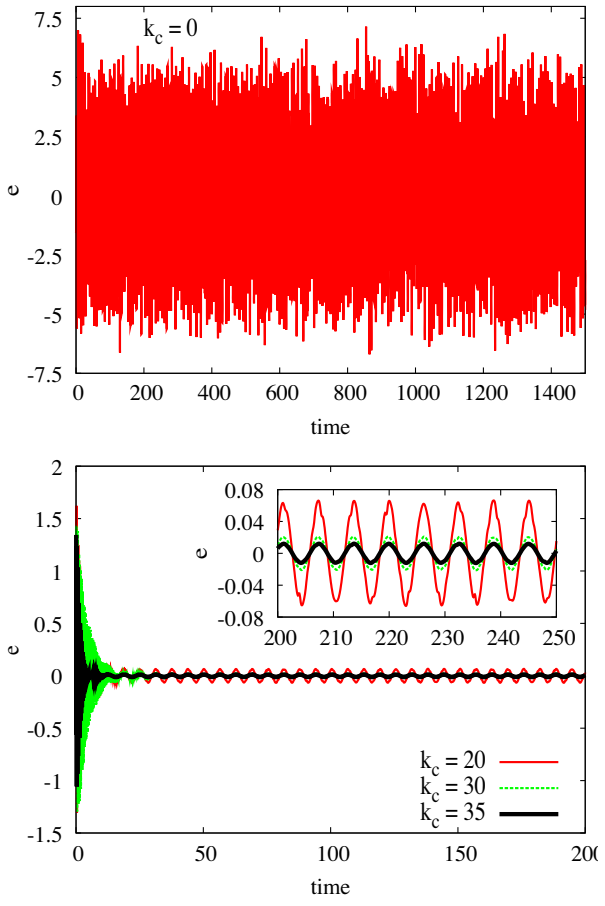

Fig. 2. Time series of the error state of system (7) and (8) for $\mu = 0.02, \omega = 1, \kappa = 3.05, \delta = 1.5, k_c = 60, F = 22$; and for different values of k_c. Upper panel, $k_c = 0$ (no synchronization) and lower panel, $k_c > 0$ (quasi-synchronization).

for four different values of k_c. In brief, for $k_c = 0$ (uncoupled case), ϵ oscillates chaotically; for $k_c = 20 < k_c^{th}, \epsilon \approx 0.065$, for $k_c = 30 < k_c^{th}$ (and in neighborhood of k_c^{th}), $\epsilon \approx 0.02$ and for $k_c = 35 > k_c^{th}, \epsilon \approx 0.01$. The behavior of ϵ for $k_c = 20, 30$ and 35 typifies quasi-synchronization as clearly depicted in the inset of Fig. 2.

The threshold coupling, k_c^{th} can be estimated from microscopy point of view. In principle, when the oscillators are synchronized, any microscopic property of the systems are equal or nearly equal; and one of such is the average bare energies [49] written as

$$h_{1,2} = \frac{1}{2}\int_0^T \frac{p_{1,2}^2}{2} + V(x_{1,2})dt, \tag{24}$$

where $p_{1,2}$ the momentum and $V(x_{1,2})$ is the potential energy. To eliminate transient effect, the computation of $h_{1,2}$ is done by ensuring that the trajectories run for a sufficiently long time, while measurement is carried out after discarding a sufficient initial transient (typically 2000 preiterates). Fig. 3 shows the computed h_1 and h_2 as functions of k_c, together with the average interaction energy, defined by

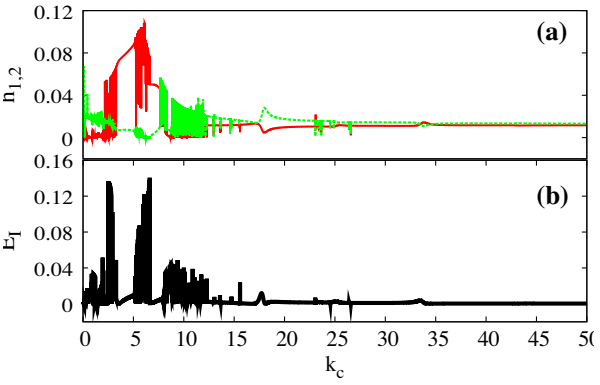

Fig. 3. (a) The average bare energies, $h_{1,2}$ *vs* k for the coupled s plasma oscillator for the parameters of Fig. 2. (b) The average interaction energies, E_I.

$$E_I(t) = \frac{1}{T}\int_0^T \frac{k}{2}(x_1 - x_2)^2 dt. \tag{25}$$

$E_I(t)$ characterizes the contributions to the total energy that is caused by an interaction, respectively. As k_c becomes increasingly large (say, $k_c^{th} > k_c^{th} \approx 23.94$), the correlation in the dynamics becomes stronger while they asymptotically approach near identical trajectories, typical of quasi-synchronization.

4. Bifurcations and attractors

In this section, we seek to examine the dynamics preceding the quasi-synchronized state of systems (7) and (8) when the control parameter, namely k_c evolves. In this regards, bifurcation diagrams and their corresponding Lyapunov exponents spectra are useful tools for numerical as well as experimental exploration studies when there is a tunable parameter, which in this case is the coupling strength k_c. When k_c varies, several new bifurcation sequences which were not observed in the singled plasma oscillator were found. For the numerical computations, k_c is increased from an initial value $k_c^i = 0.0$ to a final value $k_c^f = 50$; and then decreased from k_c^f to k_c^i. In this way, all possible attractors that may co-exist would be captured in phase space. Starting with initial conditions $(x_1, \dot{x}_1) = (0, 0.5), (x_2, \dot{x}_2) = (1.5, 2.5)$, systems (7) and (8) is again integrated using the fourth-order Runge–Kutta method. Since the extended phase space is five-dimensional ($IR^4 \times \varphi^1$), an element of the state space is denoted by $(x_1, dx_1/dt, x_2, dx_2/dt, \theta)$; φ^1 being the unit circle containing the phase angle, $\theta = \omega t$. Thus, to visualize the attractors in the subspace along with their bifurcations, we follow the same approach as in [38], by exploring the dynamics in the Poincaré cross section defined by

$$\sum = \left\{(x_1, dx_1/dt, x_2, dx_2/dt, \theta = \theta_0) \in IR^4 \times \varphi^1\right\}, \tag{26}$$

where θ_0 is a constant determining the location of the Poincaré cross section on which the coordinates $X(x_1, dx_1/dt, x_2, dx_2/dt)$ of the attractors are expressed. The simulation is carried out for 100 periods of the driving

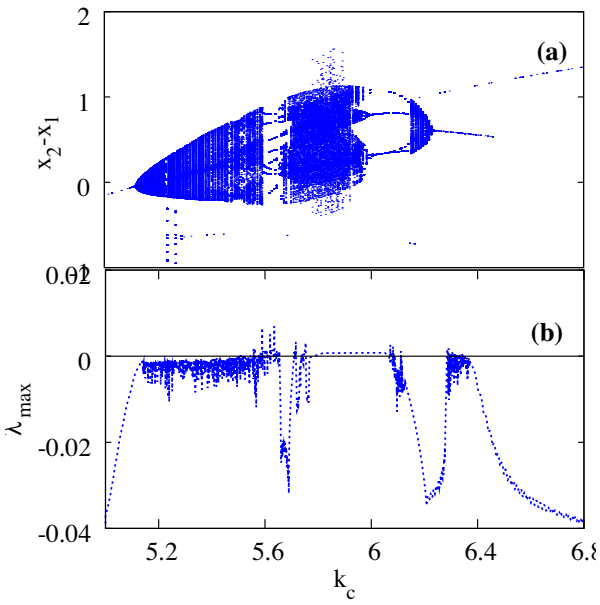

Fig. 4. (a) Bifurcation structure of the error dynamics $(x_2 - x_1)$ as a function of coupling strength k_c for $\mu = 0.02, \omega = 1, k = 3.05, \delta = 1.5$ and $F = 22.0$ in the interval $4.8 \leqslant k_c \leqslant 7.2$ (containing a bubble), (b) corresponding maximum Lyapunov exponent.

force until the transient died out, so that trajectories are attractors with insignificant local calculation error. To ensure periodic, quasiperiodic and chaotic trajectories, the system is integrated for the next 180 periods, allowing one to observe coexisting attractors evolving from different initial conditions. So the bifurcation diagrams obtained here only show the projection of attractors in the Poincaré section onto the synchronization manifold, $x_2 - x_1$ vs the control parameter, k_c.

With systems (7) and (8), we can indeed find different kinds of dynamical transitions. To illustrate the main features, we computed and examined a great number of bifurcation structures, with the corresponding Lyapunov exponent as functions of k_c in a broad range of k_c; from which we observed interesting chaotic domains, coexisting attractors, sandwiched by periodic windows made up of different periodicity (up-to period-9 orbit, where found), period-doubling (*pd*), symmetry-breaking (sb), saddle node (*SN*) and Hopf bifurcations. We present here, for brevity, in Fig. 4 a typical bifurcation diagram of the error dynamics $(x_2 - x_1)$. We have zoomed in two distinct regimes, namely $4.8 \leqslant k_c \leqslant 7.2$ (Fig. 4 enclosing a bubble) and $5.6 \leqslant k_c \leqslant 5.8$ (Fig. 6 with large period-8 window), respectively. At the left branch of Fig. 4, a period-1 attractor undergoes a Hopf bifurcation at $k_c \approx 5.12$ to a quasiperiodic orbit (Shown in Fig. 5(b)) that looses its stability at $k_c \approx 5.57$ via sudden creation of new chaotic attractors in the sub-systems at $k_c = 5.58$ (Fig. 5(b)). At $k_c \approx 5.66$ a *SN* bifurcation takes place, giving birth to a period-8 orbit that undergoes *sb* and *pd* to chaos as shown in Fig. 6, where we further zoomed the bifurcation structure where period-8 orbit is predominant. An interesting feature is the reversed sequence: creation of a period-3 attractor - chaos – quasiperiodicity – Hopf bifurcation terminated by a steady state periodic orbit; all of which are qualitatively characterized by the Lyapunov exponents. We emphasize that beside quasi-synchronization, the occurrence of Hopf bifurcation is one dominant effect of interaction on the dynamics of the systems. In fact, higher order Hopf bifurcation could show up for other values of the external forcing frequency. In particular, for $\omega = 2.0$, Hopf bifurcation arises when a period-3 orbit bifurcates as shown in Fig. 7.

5. Resonance oscillation state

In the study of dynamical systems, resonance is of fundamental importance. Interestingly, recent studies have shown that the phenomenon of resonance described by Galileo is in tandem with the synchronization observed by Huygens [7,50] three and halve decades later. In dynamical systems, resonance is said to occur when the frequency of an applied external forcing equals the natural frequency of the system, in which case the maximum energy output of the system is achieved and the amplitude of oscillation is large [51–53]. Here, we investigate the resonant behavior of coupled plasma oscillations. For this purpose, we employ the method of multiple times scales to analytically obtain the steady state of the coupled system. From Eqs. (7) and (8), the system is bidirectionally coupled and maybe rewritten as follows;

$$\begin{aligned}\ddot{x}_1 + \mu_1(1 + x_1^2)\dot{x}_1 + \omega_1^2 x_1 + \kappa_1 x_1^2 + \delta_1 x_1^3 &= k_c u + F\cos\Omega\tau,\\ \ddot{x}_2 + \mu_2(1 + x_2^2)\dot{x}_2 + \omega_2^2 x_2 + \kappa_2 x_2^2 + \delta_2 x_2^3 &= -k_c u,\end{aligned} \tag{27}$$

where $u = (x_2 - x_1)$. We set the time scales characterizing the modulation in amplitude and phase as $\tau_n = \epsilon^n \tau$(which gives $\tau_0 = \tau$, and $\tau_1 = \epsilon\tau$ corresponding to slow and fast time scales respectively). The following gives the equivalents of the corresponding differential coefficients.

$$\begin{aligned}\frac{d}{dt} &= \frac{d\tau_0}{dt}\times\frac{\partial}{\partial\tau_0} + \frac{d\tau_1}{dt}\times\frac{\partial}{\partial\tau_1} + \cdots\\ &= \frac{dt}{dt}\times\frac{\partial}{\partial\tau_0} + \frac{\epsilon dt}{dt}\times\frac{\partial}{\partial\tau_1} + \cdots, = D_0 + \epsilon D_1 + \cdots\end{aligned} \tag{28}$$

which leads to

$$\begin{aligned}\frac{d^2}{dt^2} &= (D_0 + \epsilon D_1 + \cdots)^2 = D_0^2 + 2\epsilon D_0 D_1 + \epsilon^2 D_1^2 + \cdots,\\ &= D_0^2 + 2\epsilon D_0 D_1 + \cdots\end{aligned} \tag{29}$$

We seek an approximate solution of the form:

$$\begin{aligned}x_1(t) &= x_{10}(\tau_0, \tau_1) + \epsilon x_{11}(\tau_0, \tau_1) + \cdots,\\ x_2(t) &= x_{20}(\tau_0, \tau_1) + \epsilon x_{21}(\tau_0, \tau_1) + \cdots\end{aligned} \tag{30}$$

Substituting Eqs. (28)–(30) into Eq. (27) and comparing the coefficients of the same order of ϵ, the following differential equations are obtained.

$$D_0^2 x_{10} + \omega_1^2 x_{10} = 0; \quad D_0^2 x_{20} + \omega_2^2 x_{20} = 0, \tag{31}$$

$$\begin{aligned}D_0^2 x_{11} + \omega_1^2 x_{11} = &-2D_0 D_1 x_{10} - \mu_1 D_0 x_{10} - \mu_1 x_{10}^2 D_0 x_{10} - k x_{10}^2\\ &- \delta x_{10}^3 + k_c(x_{20} - x_{10}) + F\cos\Omega\tau,\\ D_0^2 x_{21} + \omega_2^2 x_{21} = &-2D_0 D_1 x_{20} - \mu_2 D_0 x_{20} - \mu_2 x_{20}^2 D_0 x_{20}\\ &- k x_{20}^2 - \delta x_{20}^3 + k_c(x_{10} - x_{20}).\end{aligned} \tag{32}$$

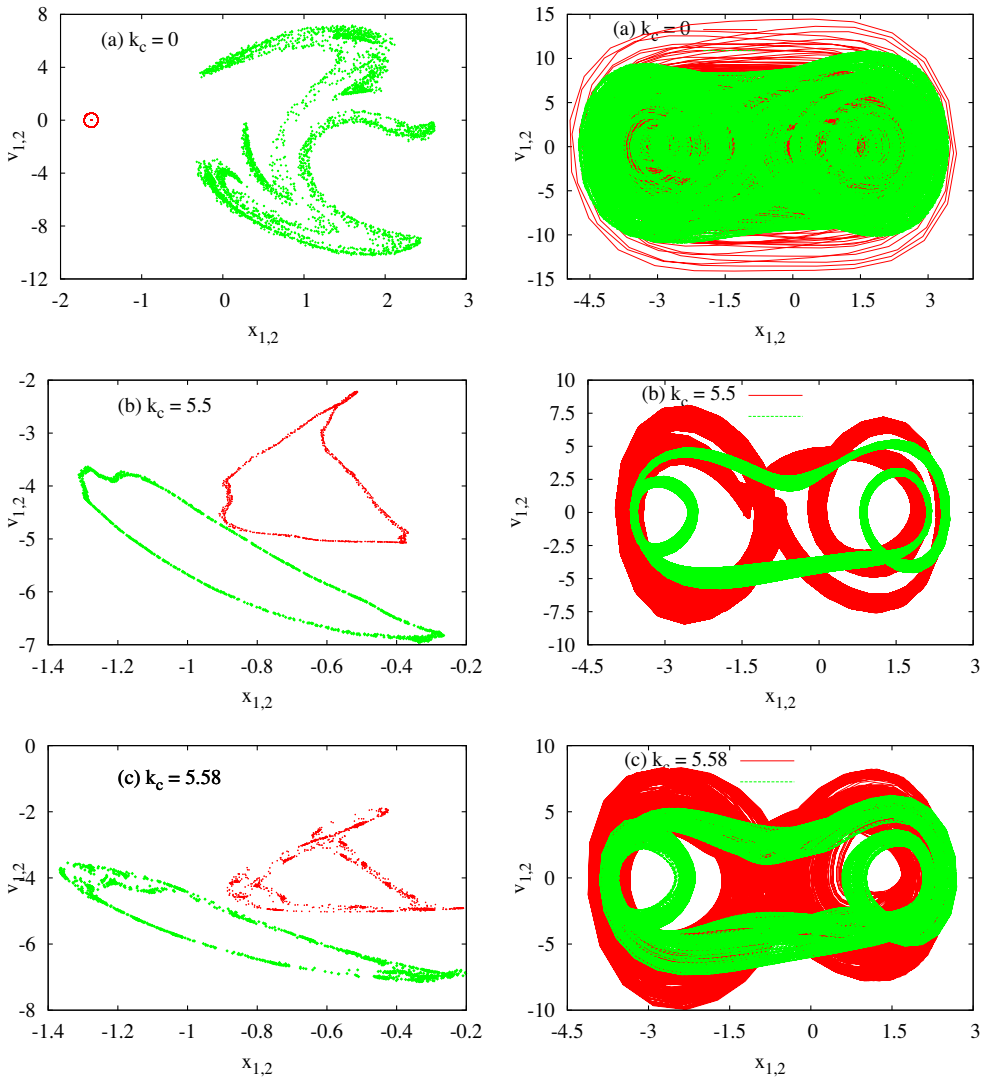

Fig. 5. Poincaré sections (left) and the corresponding phase portraits (right) for different coupling strengths, k_c. Other parameters are: $\mu = 0.02, \omega = 2.0, k = 3.05, \delta = 1.5$ and $F = 22.0$. Driven system (green), non-driven system (red). (For interpretation of the references to color in this figure caption, the reader is referred to the web version of this article.)

Here, we consider all the parameters to be of the order of the small parameter ϵ, that is $\kappa = \epsilon\kappa, \delta = \epsilon\delta, F = \epsilon F$. In addition to this, $\omega_1 \simeq \Omega$ and $\omega_1 \simeq \omega_2$; implying that $\Omega = \omega_1 + \epsilon\sigma$, where σ is the detuning parameter. Therefore, the general solution of Eq. (32) expressed in polar form is

$$x_{10} = A_1(\tau_1)e^{iw_1\tau_0} + c.c; \quad x_{20} = A_2(\tau_1)e^{iw_2\tau_0} + c.c., \tag{33}$$

where *c.c.* represents complex conjugate. By substituting Eq. (33) into Eq. (32) one obtains the first order approximation solution as

$$\begin{aligned} &2\omega_1 A_1' + \mu_1\omega_1 A_1 + \mu_1\omega_1 A_1|A_1|^2 \\ &- 3i\delta A_1|A_1|^2 + ik_c(A_2 - A_1) + \frac{i}{2}Fe^{i\sigma\tau_1} = 0. \\ &2\omega_2 A_2' + \mu_2\omega_2 A_2\left(1 + |A_2|^2\right) - 3i\delta A_2|A_2|^2 + ik_c(A_1 - A_2) = 0. \end{aligned} \tag{34}$$

We can again express A_1 and A_2 as follows:

$$A_1 = \frac{1}{2}a_1(\tau_1)e^{i\theta_1(\tau_1)}; \quad A_2 = \frac{1}{2}a_2(\tau_1)e^{i\theta_2(\tau_1)}. \tag{35}$$

Substituting Eq. (35) into Eq. (34) and separating real and imaginary parts, one obtains the following coupled first order differential equations:

$$\begin{aligned} \omega_1 a_1' &= -\frac{1}{2}\mu_1\omega_1 a_1 - \frac{1}{8}\mu_1\omega_1 a_1^3 + \frac{1}{2}k_c a_2 \sin\gamma_2 + \frac{F}{2}\sin\gamma_1, \\ \omega_1 a_1\gamma_1' &= \omega_1 a_1\sigma - \frac{3}{8}\delta a_1^3 - \frac{1}{2}k_c a_1 + \frac{1}{2}k_c a_2\cos\gamma_2 + \frac{F}{2}\cos\gamma_1, \\ \omega_2 a_2' &= -\frac{1}{2}\mu_2\omega_2 a_2\left(1 + \frac{a_2^2}{4}\right) - \frac{1}{2}k_c a_1\sin\gamma_2, \\ \omega_2 a_2\gamma_2' &= \frac{3}{8}\delta a_2^3 - \frac{1}{2}k_c a_1\cos\gamma_2 + \frac{1}{2}k_c a_2 - \omega_2 a_2(\sigma - \gamma_1'), \end{aligned} \tag{36}$$

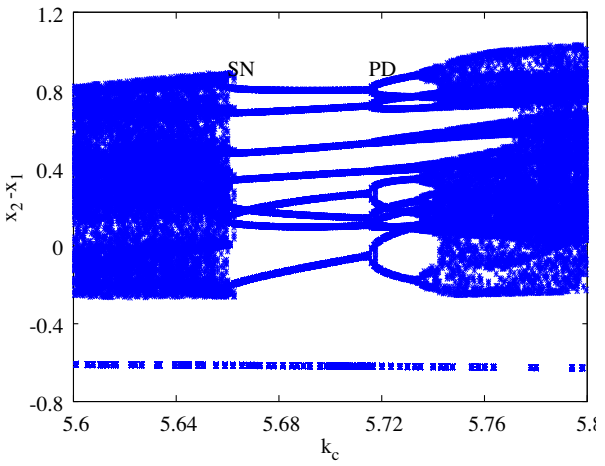

Fig. 6. Zoom of the bifurcation structure in Fig. 4 in the interval $5.6 \leqslant k_c \leqslant 5.8$ (sandwiching a period-8 attractor window) for $\mu = 0.02,\ \omega = 1,\ k = 3.05,\ \delta = 1.5$ and $F = 22.0$.

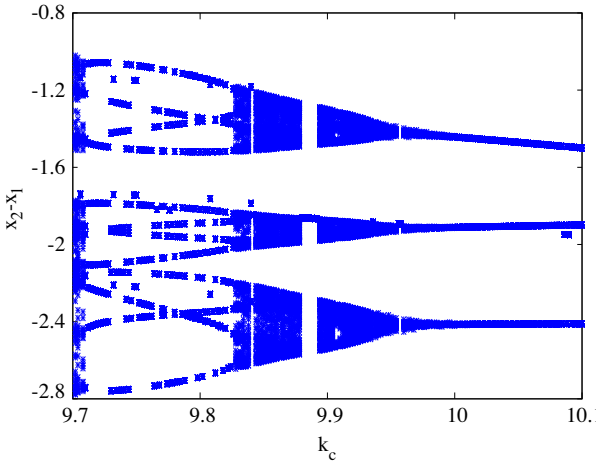

Fig. 7. Bifurcation structure of the error dynamics $(x_2 - x_1)$ as a function of coupling strength k_c for $\mu = 0.02, \omega = 2.0, k = 3.05, \delta = 1.5$ and $F = 22.0$; showing hopf bifurcations emerging from a period-3 orbit.

where $\gamma_1 = \sigma\tau_1 - \theta_1$ and $\gamma_2 = \theta_2 - \theta_1$. In the absence of coupling stiffness, that is $k_c = 0$, and $\omega_1 = \mu_2 = 1$, with $a_2 = \mu_2 = 0$, Eq. (36) reduces to Eq. (37) obtained in [30], and corresponding to single plasma oscillator model.

$$a' = -\frac{1}{2}a - \frac{3}{8}a^3 + \frac{F}{2}\sin\gamma,$$
$$a\gamma' = \sigma a - \frac{3}{8}\delta a^3 + \frac{F}{2}\cos\gamma. \tag{37}$$

We then determine the steady state motion by noting that $a_1' = a_2'$ and $\gamma_1' = \gamma_2' = 0$. Eliminating γ_1 and γ_2 and setting $\sin\gamma_2 = -\frac{\mu_2\omega_2 a_2}{k_c a_1}\left(1 + \frac{a_2^2}{4}\right)$ and $\cos\gamma_2 = \frac{1}{k_c a_1}\left(\frac{3}{4}\delta a_2^2 + k_c a_2 - \omega_2 a_2\sigma\right)$ from Eq. (14), one obtains the following set of equations:

$$\frac{F^2}{4} = \left(\frac{1}{2}\mu_1\omega_1 a_1 + \frac{1}{8}\mu_1\omega_1 a_1^3 + \frac{1}{2}\mu_2\omega_2\frac{a_2^2}{a^1}\left(1 + \frac{a_2^2}{4}\right)\right)^2 - \left(\omega_1 a_1\sigma - \frac{3}{8}\delta a_1^3 - \frac{k_c a_1}{2} + \frac{k_c a_2^2}{2} - \omega_2 a_2^2\sigma + \frac{3}{8}\delta a_2^4\right)^2, \tag{38}$$

$$\frac{1}{4}k_c^2 a_1^2 = \frac{1}{4}\omega_2^2 a_2^2\left(1 + \frac{a_2^2}{4}\right)^2 + \left(\frac{3}{8}\delta a_2^3 + \frac{1}{2}k_c a_2 - \omega_2 a_2\sigma\right)^2. \tag{39}$$

In order to examine the frequency response of the coupled plasma oscillators, the steady state equations, Eqs. (38) and (39), are numerically integrated using the fourth-order Runge–Kutta integration algorithm. The result is presented in Fig. 8 for different values of the coupling strength, k_c and fixed parameters $\mu_1 = \mu_2 = 0.4, \kappa_1 = \kappa_2 = 1.0, \delta_1 = \delta_2 = 0.3$, $\omega_1 = \omega_2 = 1.0$, and moderate forcing amplitude, $F = 0.05$. Here, we observe the existence of bi-resonance with respect to the coupling strength. Besides the dependence of the resonance peaks on the forcing frequency (Ω), two regimes of resonance emerged within the observed forcing frequency range. First, the coupling strength (k_c) was set to zero. The resonance in this case shows the highest amplitude and corresponds to that of a single periodically forced plasma system [30]. As the

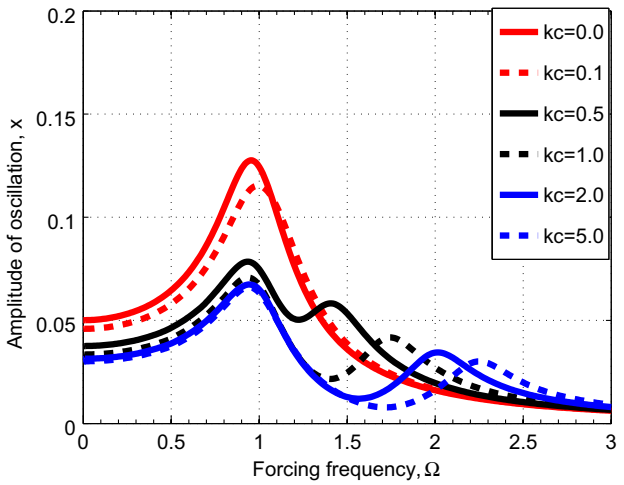

Fig. 8. The frequency response of the plasma oscillations for different values of the coupling strength, k_c.

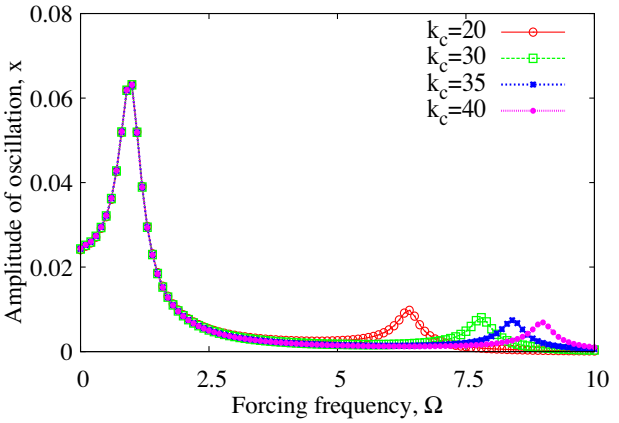

Fig. 9. The frequency response of the plasma oscillations for different values of the coupling strength, k_c in the synchronization regime.

coupling is slightly tuned such that the oscillators are weakly coupled (at $k_c = 0.1$), the vibration is comparable to the uncoupled case ($k_c = 0$); however, the interaction between the two systems depresses the resonance peak lower, so that a slightly increased resonance frequency is obtained.

With increasing coupling strength, the interaction between the two systems drives them to multi-resonance regime. Depending on parameter set, one or more resonance frequencies may appear beside the primary resonance. Notably, the resonance frequencies at which the primary resonances occurred for $k_c > 0.1$ are approximately the same. However, stronger interaction between the two systems depresses the resonance peak even much lower, so that the oscillators vibrate with lower amplitude. For $k_c \geqslant 0.5$, each curve shows two distinct resonance frequencies. The positions of the secondary resonances suggest that their resonance frequencies, as well as the amplitude of oscillations of the plasma system depend strongly on the strength of interaction between the coupled systems. When the two coupled plasma oscillators reach synchronization state as depicted in Fig. 2 for $k_c \geqslant 20$, the primary resonance frequencies and peaks coincides for all k_c in the synchronization regime. However, the secondary resonance frequencies differ for different coupling strengths with slight difference in the resonance peaks as shown in Fig. 9.

6. Conclusions

In this paper, synchronization and resonances of two coupled and periodically driven plasma oscillators have been investigated. Quasi-synchronization has been found to exist between the two coupled plasmas in the presence of an asymmetric potential, when a certain threshold is reached. In this regard, the oscillators could closely be related to practical models, in which external noise, parameter mismatch and so on [11] cause the systems to suffer from achieving full synchronization but settle for a rather realistic form of collective behavior - quasi-synchronization (imperfect complete synchronization). To ascertain the sufficient condition for stable synchronized state, linear matrix inequality (LMI) method has been employed; and it has proven to provide information regarding the threshold for the existence of a synchronized dynamics. This has been validated by numerical simulations. Notably, we have also observed that when both oscillators are independently driven, the oscillators achieves complete synchronization at much smaller synchronization threshold. Furthermore, based on the method of multiple time-scale, steady state equations for the vibration of the coupled oscillators have been obtained, and bi-resonance oscillations induced by coupling have been reported at distinct frequencies. In the synchronization regime, the primary resonance frequency and peak are the same for all k_c, whereas in other regimes the resonance peaks experience depression. Multiple resonance phenomenon is well applicable in communications. For instance, the different peaks corresponding to different resonance frequencies could be harnessed to transmit data at distinct frequencies.

Acknowledgement

UEV is supported by the Royal Society of London, through their Newton International Fellowship Alumni scheme. We acknowledge and thank all the reviewers for their constructive and critical comments that were very useful for improving the quality of this paper.

References

[1] Bleckman II. Synchronization in science and technology. New York: AMSE Press; 1988.
[2] Pikovsky A, Rosemblum M, Kurths J. Synchronization: a universal concept in nonlinear science. New York: Cambridge University Press; 2001.
[3] Nagaev RF. Dynamics of synchronizing systems. Berlin-Heidelberg: Springer-Verlag; 2003.
[4] Olusola O, Vincent U, Njah AN, Olowofela J. Bistability in coupled oscillators exhibiting synchronized dynamics. Commun Theor Phys 2010;53(5):815–24.
[5] Olusola OI, Vincent UE, Njah AN. Synchronization, multistability and basin crisis incoupled pendula. J Sound Vib 2010;329:443–56.
[6] Olusola OI, Vincent UE, Njah AN. Multi-stability and basin crisis in synchronized parametrically driven oscillators. Nonlinear Dyn 2010;62:717–27.
[7] Hugenii C. Horoloquium oscilatorium, Parisiis; 1673.

[8] Boccaletti S, Kurths J, Osipov G, Valladares D, Zhou C. The synchronization of chaotic systems. Phys Rep 2002;366:1–400.
[9] Pecora L, Carrol T. Synchronization in chaotic systems. Phys Rev Lett 1990;64:821–4.
[10] Koronovskii A, Moskalenko O, Hramov A. On the use of chaotic synchronization for secure communication. Physics-Uspekhi 2009;52(12):1213–38.
[11] Stefanski A. Determining thresholds of complete synchronization and application. Singapore: World Scientific; 2009.
[12] Rosenblum MG, Pikovsky A, Kurths J. From phase to lag synchronization in coupled chaotic oscillators. Phys Rev Lett 1997;78(22):4193–6.
[13] Huang T, Li C, Yu W, Chen G. Synchronization of delayed chaotic systems with parameter mismatches by using intermittent linear state feedback. Nonlinearity 2009;22:569–84.
[14] Astakhov V, Hasler M, Kapitaniak T, Shabunin A, Anishchenko V. Effect of parameter mismatch on the mechanism of chaos synchronization loss in coupled systems. Phys Rev E 1998;58:5620–8.
[15] Johnson G, Mar D, Carroll T, Pecora L. Synchronization and imposed bifurcations in the presence of large parameter mismatch. Phys Rev Lett 1998;80:3956–9.
[16] Jalnine A, Kim S. Characterization of the parameter-mismatching effect on the loss of chaos synchronization. Phys Rev E 2002;65:026210.
[17] Suykens JAK, Curran P, Vandewalle J, Chua L. Robust nonlinear H-infinite synchronization Lure systems. IEEE Trans Circuits Syst 1997;I(44):891.
[18] Li C, Chen G, Liao X, Fan Z. Chaos quasi-synchronization induced by impulses with parameter mismatches. Chaos 2005;16:023102.
[19] Li C, Liao X, Yang X, Huang T. Impulsive stabilization and synchronization of a class of chaotic delay systems. Chaos 2005;15(4).
[20] Vassilieva E, Pinto G, Acacio de Barros J, Suppes P. Learning pattern recognition through quasi-synchronization of phase oscillators. IEEE Trans Neural Networks 2011;22(1):84–95.
[21] Pan L, Cao J. Stochastic quasi-synchronization for delayed dynamical networks via intermittent control. Commun Nonlinear Sci Numer Simul 2012;17(3):1332–43.
[22] Huang J, Li C, Huang T, Han Q. Lag quasisynchronization of coupled delayed systems with parameter mismatch by periodically intermittent control. Nonlinear Dyn 2013;71(3):469–78.
[23] Keen BE, Fletcher WHW. Nonlinear plasma instability effects for subharmonic and harmonic forcing oscillations. J Phys A: Gen Phys 1972;5:152–65.
[24] Hur MS, Lee HJ, Lee JK. Ion–beam-driven instabilities in bounded dusty plasmas. IEEE Trans Plasma Sci 1999;27(5):1449–53.
[25] Mirandaa RA, Rempela EL, Chiana AC-L, Borotto FA. Intermittent chaos in nonlinear wave–wave interactions in space plasmas. J Atmos Solar–Terres Phys 2005;67(67):1852–8.
[26] Sheridan TE. Chaos in complex plasma. Phys Plasmas 2005;12:080701.
[27] Sheridana TE, Theisen WL. Transition to chaos in a driven dusty plasma. Phys Plasmas 2010;17:013703.
[28] Viana RL, Silva ECD, Kroet T, Caldas IL, Robert M, Sanjuán MAF. Fractal structures in nonlinear plasma physics. Philos Trans Roy Soc A 2011;369(13):371–95.
[29] Enjieu-Kadji HG, Nana-Nbendjo BR, Chabi-Orou JB, Talla PK. Nonlinear dynamics of plasma oscillations modeled by an anharmonic oscillator. Phys Plasmas 2008;15:032308.
[30] Enjieu-Kadji HG, Chabi-Orou JB, Woafo P. Regular and chaotic behaviors of plasma oscillations modeled by a modified Duffing equation. Phys Scr 2008;77:025503.
[31] Enjieu-Kadji HG, Nana-Nbendjo BR. Passive aerodynamics control of plasma instabilities. Commun Nonlinear Sci Numer Simul 2012;17:1779–94.
[32] Bezruchko B, Kuznetsov SP, Trubetskov DI. Experimental observation of stochastic self-oscillations in the electron beam-backscattered electromagnetic wave dynamic system. JETP Lett 1979;29(3):162–5.
[33] Koronovskii AA, ann MVK, Hramov AE. Formation and suppression of stationary and chaotic oscillations in a non-autonomous gyrotron backward-wave oscillator. J Commun Technol Electron 2010;55(6):638–44.
[34] Rosa JE, Ticos CM, Pardo WB, Walkenstein JA, Monti M, Kurths J. Phase synchronization in a plasma discharge driven by a chaotic signal. In: In V, Kocarev L, Boccaletti S, Gluckman BJ, Kurths J, Carroll TL, editors. AIP conference proceedings. 7th Experimental chaos conference, vol. 676. San Diego, California (USA): American Institute of Physics; 2003. p. 301–6.
[35] Filatov RA, Hramov AE, Koronovskii AA. Chaotic synchronization in coupled spatially extended beam-plasma systems. Phys Lett A 2006;358:301–8.
[36] Li Y, Liao XF, Li CD, Chen G. Impulsive synchronization of laser plasma system. Commun Theor Phys 2007;47:1067–72.
[37] Fukuyama T, Watanabe Y, Kawai Y. Experimental synchronization in coupled spatially extended systems. J Plasma Fusion Res Ser 2009;8:91–5.
[38] Vincent UE, Kenfack A. Synchronization and bifurcation structures in coupled periodically forced non-identical Duffing oscillators. Phys Scr 2008;77:1–7 [045005].
[39] Wei X, Randrianandrasana MF, Ward M, Lowe D. Nonlinear dynamics of a periodically driven duffing resonator coupled to a van der pol oscillator. Math Prob Eng 2011;2011:1–16 [248328].
[40] Huber R, Wojtkowski M, Fujimoto JG. Fourier domain mode locking (fdml): A new laser operating regime and applications for optical coherence tomography. Opt Express 2006;14(8):3225–37.
[41] Yu Y, Zhang S. The synchronization of linearly bidirectional coupled chaotic systems. Chaos Solitons Fract 2004;22:189–97.
[42] Park JH. Stability criterion for synchronization of linearly coupled unified chaotic systems. Chaos Solitons Fract 2005;23:1319–25.
[43] Wu X, Cai J, Wang M. Master–slave chaos synchronization criteria for the horizontal platform systems via linear state error feedback control. J Sound Vib 2006;295:278–387.
[44] Cai J, Wu X, Chen S. Synchronization criteria for non-autonomous chaotic systems via sinusoidal state error feedback control. Phys Scr 2007;75:379–87.
[45] Chen F, Zhang W. LMI criteria for robust chaos synchronization of a class of chaotic systems. Nonlinear Anal 2007;67:3384–93.
[46] Lu JG, Hill DJ. Global asymptotical synchronization of chaotic Lure systems using sampled data: A linear matrix inequality approach. IEEE Trans Circuits Syst-II 2008;55(6):586–90.
[47] Momeni M, Kourakis I, Moslehi-Fard M, Shukla PK. A van der pol–mathieu equation for the dynamics of dust grain charge in dusty plasmas. J Phys A: Math Theor 2002;40:F473–81.
[48] Shukla PK, Mamun AA. Introduction to dusty plasma physics. IOP Publishing Ltd; 2002.
[49] Wang X, Zhan M, Lai C-H, Gang H. Measure synchronization in coupled φ^4 hamiltonian systems. Phys Rev E 2003;67:066215.
[50] Nana-Nbendjo BR, Vincent UE, McClintock PVE. Multi-resonance and enhanced synchronization in stochastically coupled ratchets. Int J Bifurcation Chaos 2012;22(6):1250141.
[51] Eisenhammer T, Hubler A, Geisel A, Luscher E. Scaling behavior of the maximum energy exchange between coupled anharmonic oscillators. Phys Rev A 1990;41:3332–42.
[52] Wargitsch C, Hubler A. Resonance of nonlinear oscillators. Phys Rev E 1995;51(2):1508–19.
[53] Peng ZK, Lang ZQ, Billings SA. Resonances and resonant frequencies for a class of nonlinear systems. J Sound Vib 2007;300:993–1014.